

PAPER • OPEN ACCESS

Analysis of secondary motions in square duct flow

To cite this article: Davide Modesti *et al* 2018 *J. Phys.: Conf. Ser.* **1001** 012009

View the [article online](#) for updates and enhancements.

You may also like

- [Secondary laser cooling and capturing of thulium atoms in traps](#)
D.D. Sukachev, E.S. Kalganova, A.V. Sokolov et al.
- [A Method of Measuring the Axial Secular Motion Temperature of Trapping Large Size Ion Clouds](#)
Yu-Na Yang, Hao Liu et al.
- [THE ALLWISE MOTION SURVEY AND THE QUEST FOR COLD SUBDWARFS](#)
J. Davy Kirkpatrick, Adam Schneider, Sergio Fajardo-Acosta et al.



ECS
The
Electrochemical
Society
Advancing solid state &
electrochemical science & technology

DISCOVER
how sustainability
intersects with
electrochemistry & solid
state science research

Analysis of secondary motions in square duct flow

Davide Modesti¹, Sergio Pirozzoli², Paolo Orlandi² and Francesco Grasso¹

¹Cnam-Laboratoire DynFluid, 151 Boulevard de L'Hopital, 75013 Paris, France

²Dipartimento di Ingegneria Meccanica e Aerospaziale, Sapienza Università di Roma

Via Eudossiana 18, 00184 Roma, Italy

E-mail: davide.modesti@lecnam.net

Abstract. We carry out direct numerical simulations (DNS) of square duct flow spanning the friction Reynolds number range $Re_\tau^* = 150 - 1055$, to study the nature and the role of secondary motions. We preliminarily find that secondary motions are not the mere result of the time averaging procedure, but rather they are present in the instantaneous flow realizations, corresponding to large eddies persistent in both space and time. Numerical experiments have also been carried out whereby the secondary motions are suppressed, hence allowing to quantifying their effect on the mean flow field. At sufficiently high Reynolds number, secondary motions are found to increase the friction coefficient by about 3%, hence proportionally to their relative strength with respect to the bulk flow. Simulations without secondary motions are found to yield larger deviations on the mean velocity profiles from the standard law-of-the-wall, revealing that secondary motions act as a self-regulating mechanism of turbulence whereby the effect of the corners is mitigated.

1. Introduction

Flows within ducts with square cross section are the simplest prototype of internal flow with two-dimensional mean flow statistics, and they are common in many engineering applications, such as heat exchangers, turbomachinery, nuclear reactors, water draining and ventilation systems. These flows are characterized by the appearance of secondary flows, first observed by [1] and [2] who proposed their existence to explain deviations of the streamwise velocity isolines towards the corners. The topology of the secondary motions in square duct flow consists of eight counter-rotating vortices, bringing high momentum fluid from the core towards the corners. Early experimental studies on duct flow were carried out by [3, 4], reporting that the convection of mean streamwise vorticity plays an important contribution in the overall vorticity balance, whereas [4] observed that convection is at least one order of magnitude less than the other terms in the mean vorticity equation. Furthermore, [3] reported that secondary motions are not affected by the Reynolds number, whereas [4] found that their intensity decreases with Reynolds number, when scaled with the bulk duct velocity and it remains almost unchanged when scaled with the friction velocity. The same trend was also observed in the presence of rough walls [5]. From the above considerations it seems that no firm conclusions have been drawn from experiments, hence direct numerical simulation (DNS) may be a valuable tool to shed light on the role of secondary motions. A first DNS of incompressible duct flow was performed by [6] at $Re_b = 4410$ ($Re_b = 2hu_b/\nu$, where h is the duct half side, u_b the bulk velocity and ν the kinematic viscosity), corresponding to a mean friction Reynolds number of $Re_\tau^* = 150$, where $Re_\tau = hu_\tau^*/\nu$, $u_\tau^* = \sqrt{\tau_w^*/\rho_w^*}$, with τ_w^* and ρ_w^* the mean viscous stress and density at the wall, respectively. The author found that convective terms in the mean vorticity equation are negligible with respect



Table 1. Flow parameters for square duct DNS. The box dimension is $6\pi h \times 2h \times 2h$ for all flow cases. $Re_b = 2hu_b/\nu$ is the bulk Reynolds number, and $Re_\tau^* = hu_\tau^*/\nu$ is the friction Reynolds number. Δx is the mesh spacing in the streamwise direction, and Δz , Δy_w are the maximum and minimum mesh spacings in the cross-stream direction, all given in global wall-units, $\delta_v^* = \nu/u_\tau^*$. Δt_{av}^* is the effective averaging time interval. χ indicates the relative standard deviation of the wall shear stress, $\chi = \overline{(\tau_w - \tau_w^*)^2}^{1/2}/\tau_w^*$. Flow cases denoted with the 1 suffix are carried out by suppressing the secondary motions.

Case	Re_b	Re_τ^*	$C_f \times 10^3$	χ	N_x	N_y	N_z	Δx^*	Δz^*	Δy_w^*	$\Delta t_{av}^* u_\tau^*/h$
A	4410	150	9.26	0.239	512	128	128	5.6	3.0	0.55	2120
A1	4410	154	9.76	0.290	512	128	128	5.7	3.4	0.56	1049
B	7000	227	8.41	0.213	640	144	144	6.6	4.8	0.51	1607
B1	7000	230	8.64	0.265	640	144	144	6.7	4.5	0.52	120
C	17800	519	6.80	0.161	1024	256	256	9.5	6.3	0.53	1387
C1	17800	511	6.59	0.219	1024	256	256	9.4	6.1	0.65	144
D	40000	1055	5.57	0.126	2048	512	512	9.6	6.4	0.60	531
D1	40000	1038	5.39	0.212	2048	512	512	9.55	6.37	0.59	29

to the other, whereas gradients of the Reynolds stresses have the same order of magnitude but opposite sign, and their difference is balanced by viscous diffusion. [7, 8] used a spectral solver to study transition in square duct flow, spanning friction Reynolds number from laminar values up to $Re_\tau^* = 150$ and observed that a very long averaging time is necessary to collect reliable mean flow statistics ($\Delta t_{av} u_b/h = 8000$). They found that, at low Reynolds number, short-time averaging gives rise to four counter-rotating eddies, rather than eight. [9] carried out DNS of square duct flow up to $Re_\tau^* = 600$, and found that below $Re_\tau^* = 300$ low-Reynolds-number effects are particularly important. Moreover, they observed a continuous trend in the position of the secondary eddies centers, which move towards the wall bisectors as the Reynolds number increases. DNS and LES of hexagonal duct flow up to $Re_\tau^* \approx 500$ showed similar trends with the Reynolds number, namely the eddies centers move towards the duct center [10]. Even though considerable efforts have been devoted to the understanding of secondary motions, a clear picture of the phenomenon is still lacking. To further clarify the role of these motions and the effect of Reynolds number, the present authors [11] carried out DNS of square duct flow up to friction Reynolds number $Re_\tau^* = 1055$, the highest value reached so far. The results show that secondary motions scale reasonably well with the bulk flow velocity, and their net effect on the friction coefficient is rather small, and it can be effectively taken into account by introducing the hydraulic diameter. In the present work we focus on the nature of secondary motions and their existence in the instantaneous flow field. We also perform numerical experiments whereby the mean cross-flow velocities are artificially suppressed, in order to quantify their effects on the mean flow statistics and on skin friction.

2. Methodology

The compressible Navier-Stokes equations are solved, using a fourth order co-located finite difference solver, in which the convective terms are discretized using an energy-conserving scheme, which allows to preserve total kinetic energy from convection in the inviscid limit [13]. Viscous terms are expanded to Laplacian form and discretized using standard central finite difference approximations. A novel semi-implicit algorithm is used for time advancement, in order to relax the acoustic time step limitation, thus allowing to use efficiently the same solver at all Mach numbers [14]. The streamwise momentum equation is forced in such a way to

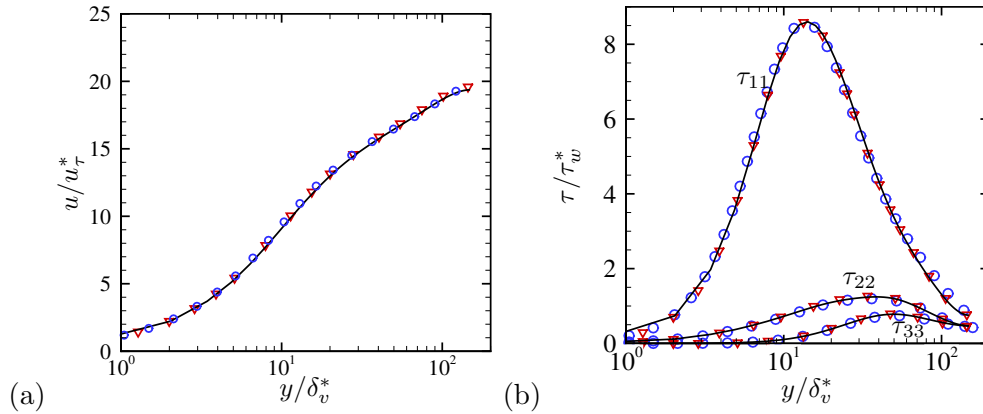


Figure 1. Profiles of mean velocity (a) and turbulent normal stresses (b) along wall bisector for flow case A (lines), compared to DNS data of [8] (triangles) at $Re_\tau = 150$, and [12] (circles) at $Re_\tau = 164$.

maintain a constant mass flow rate, periodicity is exploited in the streamwise direction, whereas isothermal no-slip boundary conditions are used at the walls [15]. In the following we denote the velocity components in the streamwise and wall-normal directions as u , v , w , respectively, whereas the overline symbol is used to indicate statistical averages in the streamwise direction and in time. We denote the local friction velocity as $u_\tau = \sqrt{\tau_w/\rho_w}$, with τ_w and ρ_w the local wall shear stress and local density at the wall; $\delta_v = \nu/u_\tau$ is the local viscous length scale and $Re_\tau = hu_\tau/\nu$ the local friction Reynolds number. Quantities normalized to local and global wall-units are denoted with a + and a * superscript, respectively. Four simulations at bulk Mach number $M_b = 0.2$ have been carried out in the range $Re_\tau^* = 150 - 1000$, and labeled as A-D (see table 1). The database is representative of incompressible turbulence, as the friction Mach number $M_\tau = u_\tau/c_w$ nowhere exceeds 0.01. Excellent agreement between the flow statistics of case A and previous DNS studies [8, 12] is observed (see figure 1).

Additional numerical experiments have been carried out at the same bulk Reynolds numbers as the baseline cases (and denoted with the 1 suffix), by artificially suppressing the secondary motions. For that purpose, at each Runge-Kutta sub-step we force the streamwise-averaged cross-stream velocity components and to have zero mean, by setting

$$v(x, y, z, t) \rightarrow v(x, y, z, t) - \overline{v}^x(y, z, t) \quad (1a)$$

$$w(x, y, z, t) \rightarrow w(x, y, z, t) - \overline{w}^x(y, z, t), \quad (1b)$$

where $\overline{(\cdot)}^x$ denotes the streamwise averaging operator. Although the modified velocity field does not exactly satisfy the Navier-Stokes equations, we use the resulting statistics to understand the role of secondary motions, and to quantify their effect on the mean flow field. Previous studies [8, 12] highlighted the need for very long averaging time, thus we collected flow statistics for equivalent times $\Delta t_{av}^* = \Delta t_{av} L_x/(6h)$, which are considerably longer than in classical plane channel flow. On the other hand the numerical experiments carried out without secondary motions requires much shorter time averaging interval as a results of the suppression of the very slow dynamics associated with the secondary flows.

3. Secondary motions as coherent structures

Coherent structures in wall-bounded flows have been widely studied for more than a decade, but their mathematical definition is still controversial [16, 17, 18, 19]. They are usually defined

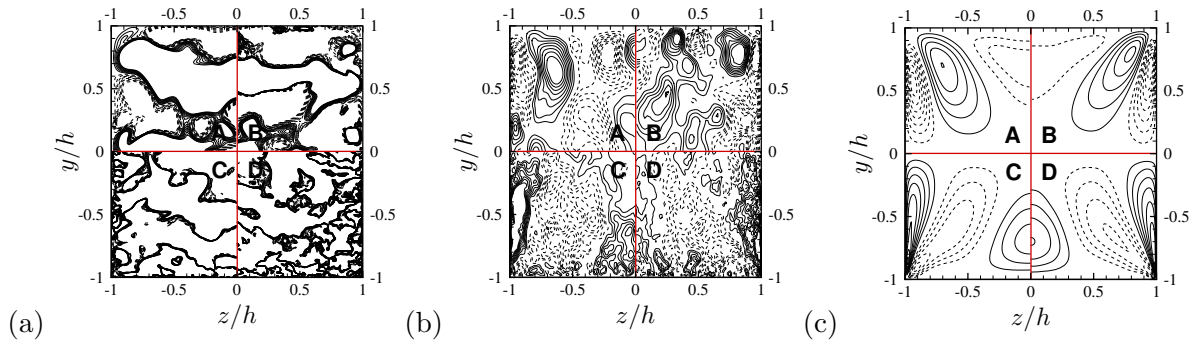


Figure 2. Distributions of vertical velocity v in the cross-stream plane: (a) instantaneous, v/u_b (b); (b) averaged in streamwise direction, \bar{v}^x/u_b (c); (c) averaged in x and time, \bar{v}/u_b . Data are reported for flow case A (top left), B (top right), C (bottom left), D (bottom right). Contour levels are shown for $-0.02 \leq (.)/(u_b) \leq 0.02$, in intervals of 0.0025 (dashed lines indicate negative values).

as flow structures which are persistent in time and space, and in this sense secondary motions in duct flow can certainly be classified as coherent, as they appear in long-time averages. On the other hand, previous studies have questioned the existence of secondary motions in the instantaneous flow field and raised the point that they may be simply the result of the averaging procedure [7, 20]. Indeed, short-time averages of low Reynolds number simulations [7] showed a topology consisting of four vortices, rather than eight, the latter only observed after long-time averaging. More recently, experiments of supersonic flow in a square duct [20] also confirmed that secondary motions are not observed in instantaneous flow visualization, but they only appear in long-time averaging or when using ad-hoc eduction techniques. figure 2 shows instantaneous, streamwise averaged and time averaged vertical velocity component. No order is found in the instantaneous cross-stream flow visualization (panel (a)), in which turbulent fluctuations high intensity comparable to u_b . Averaging the instantaneous three-dimensional field in the streamwise direction only (figure 2c), allows to filter out the incoherent turbulent fluctuations, thus selecting structures which are persistent in space. Indeed, panel (b) of figure 2 shows a more organized structure with a three-lobe arrangement, which is similar to that found in time-averaged fields (panel (c)). This observation suggests that secondary motions are persistent flow structures, since averaging in the streamwise direction only is sufficient to recover a velocity distribution that closely resemble the one found after long-time averaging.

4. The role of secondary motions

The role and the effects of secondary motions are here investigated by comparing the DNS dataset (flow cases A-D) with the numerical experiments with suppression of the secondary motions (flow cases A1-D1). In figure 3 we show the streamwise velocity in the cross-stream plane for all flow cases. By suppressing secondary motions, momentum transfer from the duct core towards the corners is inhibited, and the flow no longer exhibits the typical bulging of the velocity isolines. To further elucidate this mechanism, in figure 4 we show the various contributions to the mean streamwise momentum balance equation,

$$\underbrace{\bar{v} \frac{\partial \bar{u}}{\partial y} + \bar{w} \frac{\partial \bar{u}}{\partial z}}_C = - \underbrace{\frac{\partial \overline{u'v'}}{\partial y} - \frac{\partial \overline{u'w'}}{\partial z}}_T + \underbrace{\nu \left(\frac{\partial^2 \bar{u}}{\partial y^2} + \frac{\partial^2 \bar{u}}{\partial z^2} \right)}_V - \bar{\Pi}, \quad (2)$$

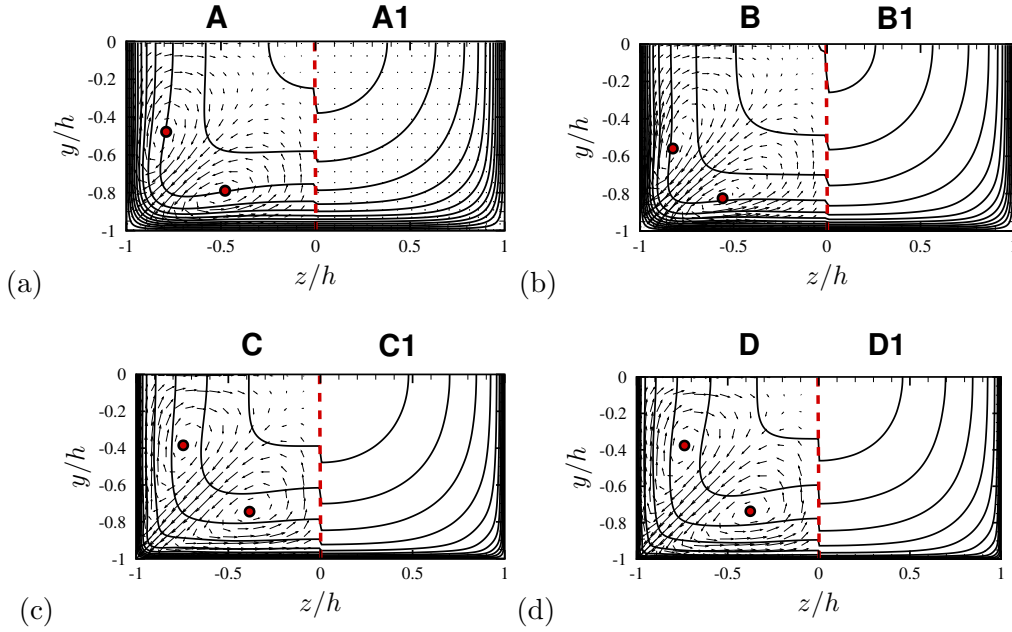


Figure 3. Mean streamwise velocity in the cross-stream plane with (left) and without (right) secondary motions for flow cases A-A1 (a), B-B1 (b), C-C1 (c) and D-D1 (d). 13 isolevels are shown in the range $0 \leq \bar{u}/(u_b) \leq 1.3$. Cross-stream velocity vectors are also shown and red circles indicate the position of the secondary eddies centers.

where C , T and V represent the contributions of mean convection, turbulence stresses and viscous diffusion, respectively, and Π is the driving pressure gradient. Mean convection (figure 4a-b) is only important in the corner proximity ($y^* \sim 150$ wall units), whereas away from the corners turbulent stresses are balanced by viscous diffusion and turbulent stresses gradients (figure 4c-f). We note that diffusion is only slightly affected by suppression of the secondary motions, whereas the turbulent stresses which balance mean convection away from walls are substantially altered (see figure 4a-b).

The wall shear stress distributions are shown in figure 5. Secondary motions are found to generally increase the wall shear stress near the corners by depleting the core region, and as consequence the distributions for cases A-D are flatter than for cases A1-D1. This effect is quantified through the relative standard deviation of the wall shear stress $\chi = \overline{(\tau_w - \tau_w^*)^2}^{1/2} / \tau_w^*$ (see table 1), which is significantly lower in the full DNS. The likely reason for this behavior is the local thinning of the wall layer in the corner proximity owing to the inward momentum flux from the duct core, and thickening as the duct mid-point is reached because of the return flow. Because of the secondary motions a peak of τ_w forms close to the corners, at a distance which well scales in wall units (about $40\delta_v^*$). As a consequence, the profiles of τ_w become flatter and flatter as Re is increased. The duct resistance coefficient is shown in table 1, and compared with the friction law for circular pipe flow in figure 6. The results show that inhibiting momentum transfer from the core towards the corner results in drag increase for flow cases A1-B1 and in drag decrease for flow cases C1-D1. This could be anticipated from figure 5, which shows that for flow cases A and B the friction increase near corners is more than compensated by friction relief along the duct perimeter, whereas the opposite happens for flow cases C, D. We argue that this behavior may be due to the non-monotonic displacement of the center of the secondary eddies, in turn associated with post-transitional effects at the lower Reynolds numbers under

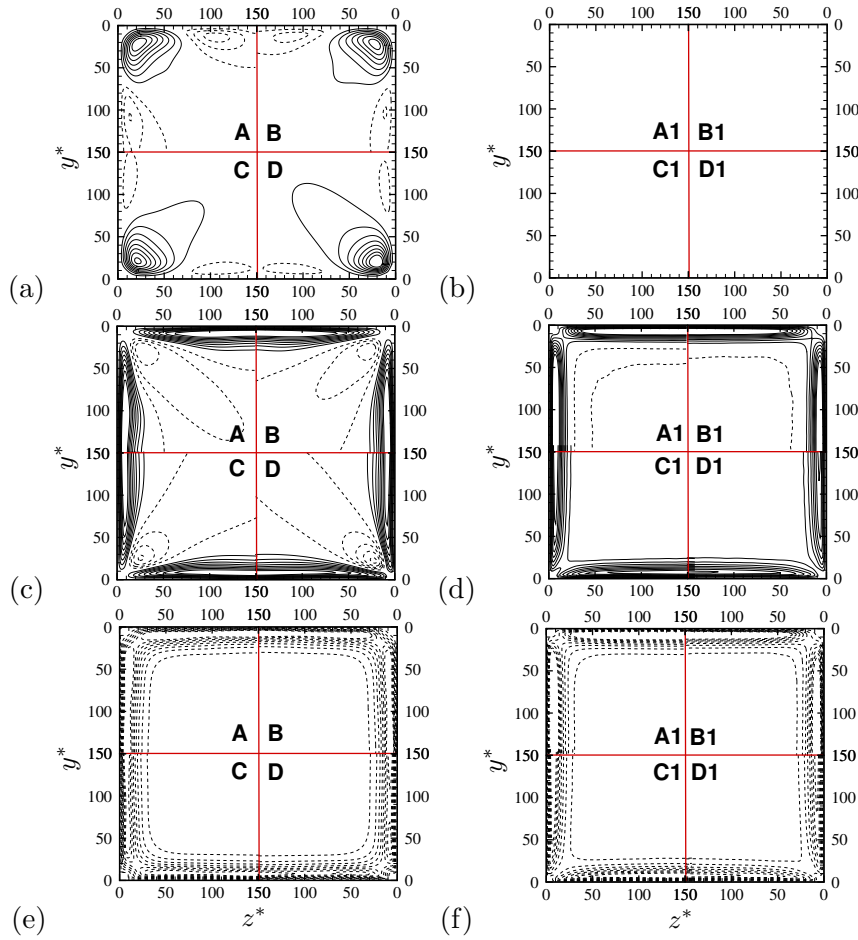


Figure 4. Terms in the mean streamwise momentum balance equation (2): convection (a-b), turbulence (c-d), viscous diffusion (e-f), with (left column) and without (right column) secondary motions. Contour levels are shown for $-0.05 \leq (\cdot)/(u_{\tau}^{*2}/\delta_v^*)^2 \leq 0.05$, in intervals of 0.005 (dashed lines denote negative values). Contour are shown for flow case A/A1 (top left), B/B1 (top right), C/C1 (bottom left), D/D1 (bottom right).

investigation (see figure 3, and consult [11]). In any case, the effect of the secondary motions on the total resistance seem to be rather small, and it may be quantified in about 3% drag increase at moderate Reynolds number, hence proportionate to their relative intensity of the secondary eddies with respect to the bulk flow.

In [11] we found that the mean velocity profiles in duct flow satisfy with good accuracy the standard law-of-the-wall up to the corner bisector. In figure 7 we show the mean streamwise velocity profiles scaled in local inner units at all z , up to $y = z$. The circular pipe flow data by [22] are also included for comparison. The figure shows that at low Reynolds number secondary motions affect the entire velocity distribution (figure 7a-b), whereas at higher Re their influence is confined to the near-wall region (figure 7c-d). The effect of secondary motions on the mean streamwise velocity is therefore limited to a distance of about 150 viscous units from the wall, which is consistent with the range of influence of the mean convection terms in the streamwise velocity budget (see figure 4a-b). We further note that the mean velocity profile of DNS is closer to the canonical profile of pipe flow as compared to cases A1-D1. Consistent with the

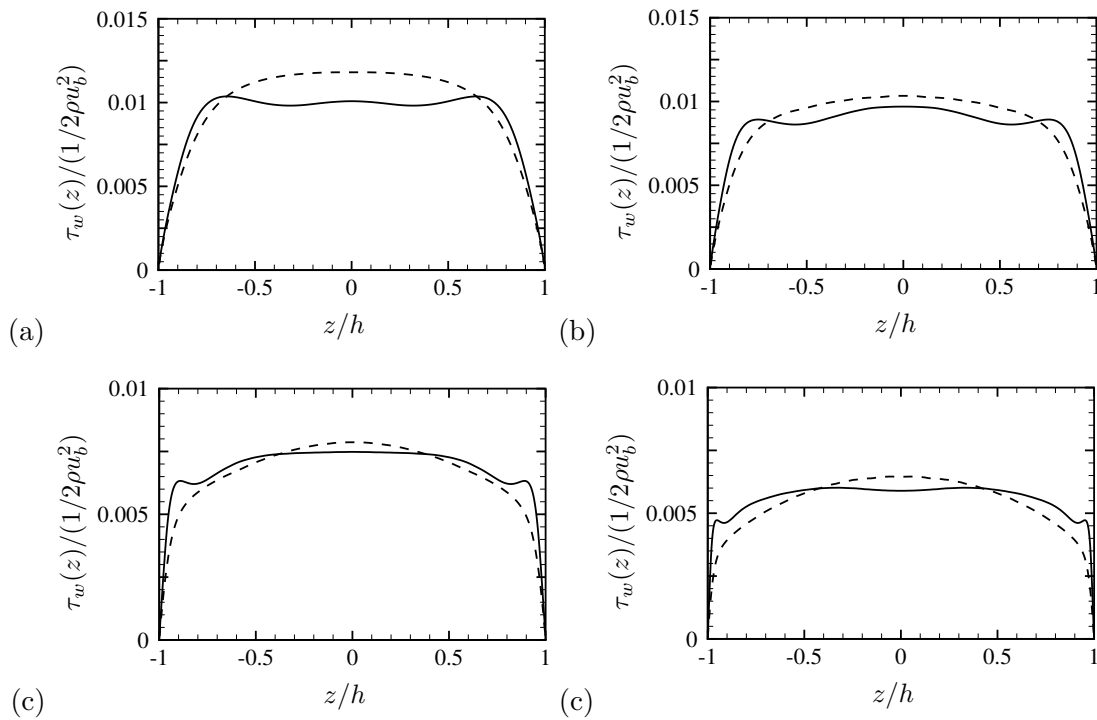


Figure 5. Mean wall shear stress distribution for DNS data (solid lines) and DNS with secondary motions suppressed (dashed lines). Flow cases A-A1 (a), B-B1 (b), C-C1 (c), D-D1 (d).

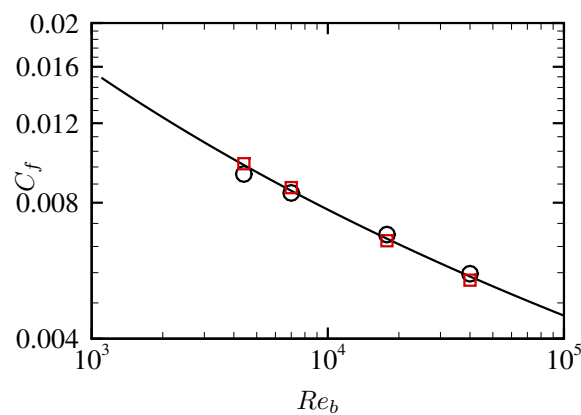


Figure 6. Friction coefficient as a function of bulk Reynolds number for DNS data (circles) and DNS with secondary motions suppressed (squares), compared with reference friction coefficient for circular pipe flow.

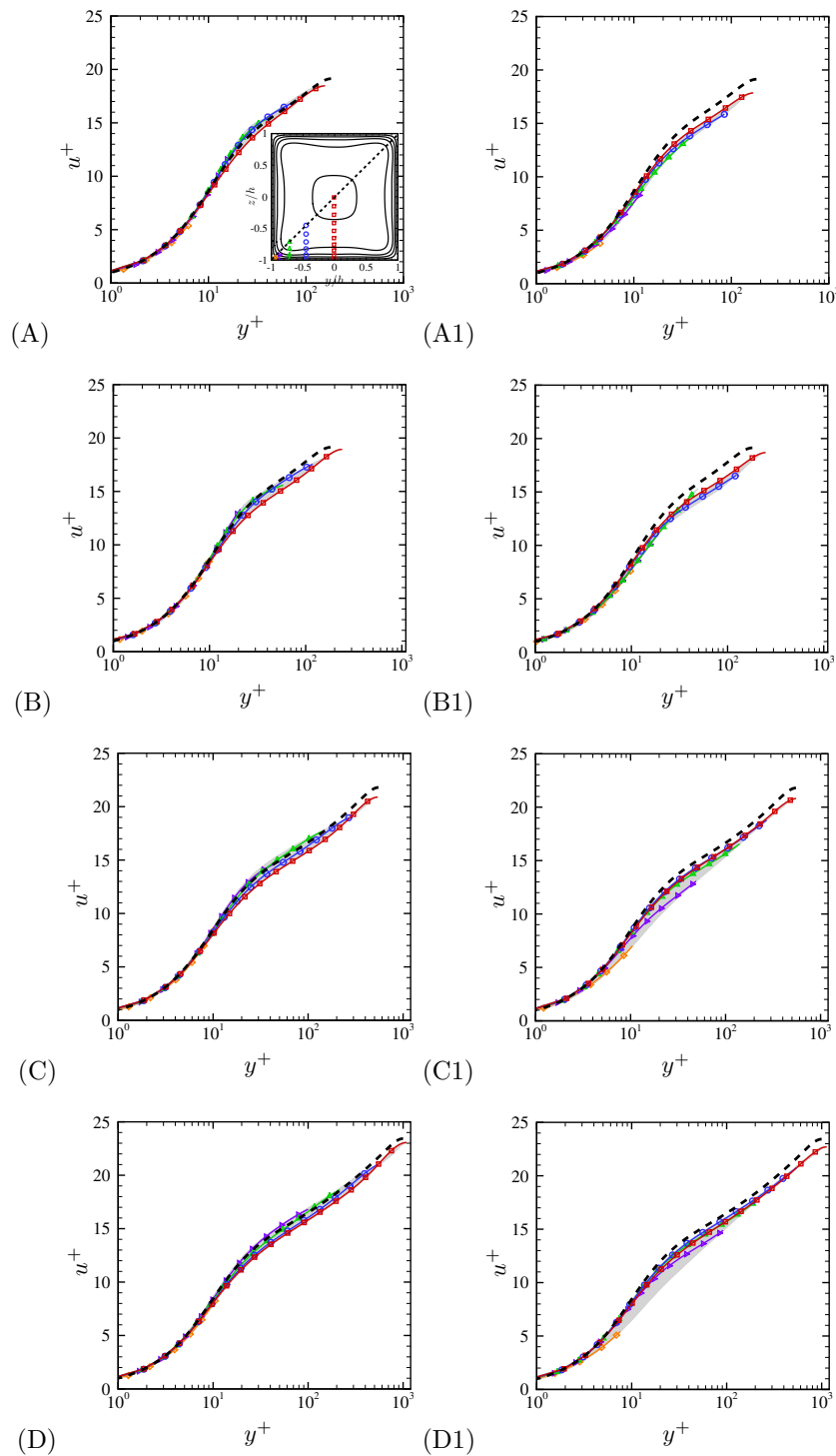


Figure 7. Mean streamwise velocity profiles along the y direction (up to the corner bisector), given in local wall-units at all z . Representative stations along the bottom wall are highlighted, namely $(z+h) = 15\delta_v^*$ (diamonds), $(z+h)/h = 0.1$ (right triangles), $(z+h)/h = 0.25$ (triangles), $(z+h)/h = 0.5$ (circles), $(z+h)/h = 1$ (squares). The dashed lines denote profiles from DNS of pipe flow flow at $Re_\tau = 140$ (A-A1) [21], $Re_\tau = 180$ (B-B1), $Re_\tau = 500$ (C-C1), $Re_\tau = 1000$ (D-D1) [22]. The inset in flow case A shows the mean streamwise velocity in the cross-stream plane with symbols denoting representative sections.

previous observations related to the flatness of the wall shear stress, this observation leads to the conclusion that the effect of mean convection associated with the secondary motions is to try to restore strict wall scaling all along the duct periphery.

5. Conclusions

We have performed DNS of square duct flow up to friction Reynolds number $Re_\tau = 1055$ to shed light on the effect of Reynolds number on secondary motions and clarify their effect on the mean flow field. We showed that, at moderate Reynolds number, averaging in the streamwise direction is sufficient to filter out the incoherent part of the velocity fluctuation, and a secondary circulation emerges which has the same spatial organization as found from long-time averaging. This observation leads to conclude that, other than being statistical artifacts, secondary motions exist in the instantaneous flow fields, although they are difficult to visualize as their intensity is smaller than the typical turbulent fluctuations. The role of the secondary motions is quantified through comparison with numerical experiments in which secondary motions are artificially suppressed. We have found that the main effect of secondary motions is to redistribute momentum from the core towards the corner, thus causing a flattening of the mean wall shear stress, which is more evident as the Reynolds number increases. The overall effect on the duct resistance coefficient is however quite small and at moderate Reynolds number secondary motions are found to increase friction of about 3%, which is proportionate to their intensity. It is especially interesting that, in the absence of mean cross-stream flow, larger deviations of the DNS data from the law-of-the-wall are observed, hence it seems that secondary motions play the role of a self-regulatory mechanism whereby the effect of the corners is mitigated, and the velocity distributions are brought back toward a universal distribution as predicted by the wall law.

Acknowledgments

We thank Miguel P. Encinar for being our host during the Third Madrid Turbulence Workshop, funded by the COTURB project of the European Research Council, and Prof. J. Jiménez for the invitation. We wish to thank Prof. A. Pinelli and Dr. R. Vinuesa for sharing their DNS data. We further acknowledge that most of the results reported in this paper have been achieved using the PRACE Research Infrastructure resource MARCONI based at CINECA, Casalecchio di Reno, Italy. We are finally grateful to Marco Atzori for his careful review of the manuscript.

References

- [1] Nikuradse J 1926 *Untersuchung über die Geschwindigkeitsverteilung in turbulenten Strömungen* (Vdi-verlag)
- [2] Prandtl L 1927 *Reports of the Aerod. Versuchsanst, Göttingen, Germany, 3rd Series*
- [3] Brundrett E and Baines W 1964 *J. Fluid Mech.* **19** 375–394
- [4] Gessner F and Jones J 1965 *J. Fluid Mech.* **23** 689–713
- [5] Launder B and Ying W 1972 *J. Fluid Mech.* **54** 289–295
- [6] Gavrilakis S 1992 *J. Fluid Mech.* **244** 101–129
- [7] Uhlmann M, Pinelli A, Kawahara G and Sekimoto A 2007 *J. Fluid Mech.* **588** 153–162
- [8] Pinelli A, Uhlmann M, Sekimoto A and Kawahara G 2010 *J. Fluid Mech.* **644** 107–122
- [9] Zhang H, Trias F, Gorobets A, Tan Y and Oliva A 2015 *Int. J. Heat Fluid Flow* **54** 258–267
- [10] Marin O, Vinuesa R, Obabko A and Schlatter P 2016 *Phys. Fluids* **28** 125101
- [11] Pirozzoli S, Modesti D, Orlandi P and Grasso F 2017 *arXiv preprint arXiv:1707.03638*
- [12] Vinuesa R, Noorani A, Lozano-Durán A, El Khoury G, Schlatter P, Fischer P and Nagib H 2014 *J. Turbul.* **15** 677–706
- [13] Pirozzoli S 2010 *J. Comput Phys.* **229** 7180–7190
- [14] Modesti D and Pirozzoli S 2017 *J. Sci. Comput.* URL <https://doi.org/10.1007/s10915-017-0534-4>
- [15] Modesti D and Pirozzoli S 2016 *Int. J. Heat Fluid Flow* **59** 33–49
- [16] Townsend A 1976 *The structure of turbulent shear flow* (Cambridge U. Press)
- [17] Sharma A and McKeon B 2013 *J. Fluid Mech.* **728** 196–238
- [18] Adrian R and Marusic I 2012 *J. Hyd. Res.* **50** 451–464

- [19] Lozano-Durán A and Jiménez J 2014 *J. Fluid Mech.* **759** 432–471
- [20] Morajkar R and Gamba M 2016 *54th AIAA Aerospace Sciences Meeting* p 1590
- [21] Verzicco R and Orlandi P 1996 *J. Comput. Phys.* **123** 402–414
- [22] El Khoury J, Schlatter P, Noorani A, Fischer P, Brethouwer G and Johansson A 2013 *Flow Turbul. Combust.* **91** 475–495